Spectropolarimetric imaging for pathological analysis of skin

Yongqiang Zhao,[1,*] Lei Zhang,[2] and Quan Pan[1]

[1]College of Automation, Northwestern Polytechnical University, Xi'an 710072, China

[2]Department of Computing, The Hong Kong Polytechnic University, Hong Kong, China

*Corresponding author: zhaoyq@nwpu.edu.cn

Received 4 September 2008; revised 27 January 2009; accepted 4 February 2009; posted 6 February 2009 (Doc. ID 100813); published 4 March 2009

Pathological changes of skin will change the tissue's birefringence and structure, which can be measured by the polarization and spectral changes of the tissue's scattering light. Light-scattering spectropolarimetry is an effective tool to measure these features for quantitative pathology analysis. An epithelial tissue imaging spectropolarimeter is proposed to acquire the spectral, polarimetric, and spatial characteristic changes of the tissue, and then a spectropolarimetric correction method is proposed to compute the tissue's polarimetric spectrum, which can be used for pathological analysis of tissue. Finally, to aid doctors for more accurate clinical diagnosis, a false color mapping based spectropolarimetric image fusion method is proposed to enhance the visual differences between normal skin and pathological skin. Experimental results demonstrate the potential of the proposed techniques for pathological diagnosis and treatment evaluation of skin.

OCIS codes: 170.6510, 260.5430, 100.2980, 100.5010.

1. Introduction

Noninvasive medical imaging for highly scattering biological tissue such as human skin is an important problem in biomedical science. Recent advances in molecular and optical techniques have led to a new horizon of biomedical imaging to measure the rich amount of biochemical and structural information contained in the optical signatures of tissues. The various forms of skin pathology exhibit some common morphological changes and molecular changes on microscopic examination [1]. The nuclei can become enlarged, pleomorphic (irregular in contour and size distribution), "crowded" (occupy more of the tissue volume), and hyperchromatic (stain more intensely with nuclear stains) [1–3]. All these changes will affect the tissue birefringence and structure. Scattered light from tissue can provide important information about these changes [1–12].

Light-scattering spectroscopy has been extensively used in physical science to study a variety of materials [13]. Although biological tissue is different from mineral, it can also be studied with a light-scattering spectrum. It has been demonstrated that the light-scattering spectrum can provide structural and functional information about biological tissues [1,2,7–10]. When linearly polarized light propagates through biological tissue, it will be rapidly depolarized by birefringent collagen fibers [3–5]. The polarization states of the scattered light can be used to describe the birefringence information about the biological tissue.

Considering that the light-scattering spectra and polarization states can provide quantitative, objective information on pathological parameters in real time without tissue removal, Gurjar *et al.* [2] developed a new biomedical imaging modality based on polarized light-scattering spectroscopy to measure morphological information about epithelial cells *in situ*. Backman *et al.* [1] used polarized light-scattering spectroscopy to quantitatively measure epithelial cellular structures *in situ*. Jacques *et al.*

0003-6935/09/10D236-11$15.00/0

[5] used polarized light for superficial tissue imaging. In this study we will show that, by simply collecting two polarization images through aligned and crossed polarizers and then computing the degree of linear polarization, the image contrast could be significantly improved, and thus the superficial skin structures can be enhanced for better visual inspection. Jarry *et al.* [12] studied the randomization of linearly polarized light as it propagates through tissues and microsphere solutions, observing a surprising persistence of polarization when light propagates through liver tissues despite multiple scattering of photons. However that work either utilized the spectral information in a single polarization angle or utilized the polarimetric information in a single band. According to the image chain theory [14], by exploiting more information about the object of interest, better identification performance can be obtained. If polarization and spectral information can be effectively used to describe skin pathology, more accurate analysis can be expected.

The introduction of imaging spectropolarimetry makes it possible to combine the spectral, polarimetric, and spatial information. The computational methods originally developed for solving remote sensing problems have been adapted and modified for biomedical applications. Considering the spectral and polarimetric variations for different biological tissue states, an imaging spectropolarimeter could be used to improve the capability of automated systems for biological tissue analysis. Skin is the largest organ of the human body, and the interaction between skin and light often involves localized or diffuse changes in spectra and polarization states. A better understanding of mechanisms of such interactions is therefore critical to the study of skin physiology and pathology. Here we focus on the use of a spectropolarimetric imaging method to analyze the optical characteristics of skin. We first present a stable, wide-field, spectropolarimetric imaging system that can measure 2D spatial, spectral, and polarimetric information simultaneously. In order for a unified representation of the polarimetric reflectance, a spectropolarimetric correction method is proposed to compute the tissue's polarimetric spectrum, which is necessary to quantitatively analyze the tissue pathological information. According to the characteristics of spectropolarimetric imagery of skin in different pathological conditions, a false color mapping based spectropolarimetric imagery fusion method is proposed to enhance the pathological region.

2. Materials and Methods

A. Spectropolarimetry

This section briefly introduces the basic concepts of spectropolarimetry. For more information about spectropolarimetry, please refer to [15]. The polarization of a monochromatic beam is fully characterized by a four-element Stokes vector $[S_0, S_1, S_2, S_3]$. Considering that the fourth term S_3 (i.e., the circular state) requires the introduction of a wave plate, which makes the instrument more complicated, and that the value of S_3 is far below that of the other three elements in most imaging processes, usually only the first three terms of the Stokes vector, i.e., $[S_0, S_1, S_2, S_3]$, are used to characterize the linear portion of a beam.

We describe a beam of monochromatic and linear polarized radiation emitted or reflected from a tissue surface by the first three Stokes parameters $S = [S_0, S_1, S_2]$, The three parameters S_0, S_1, and S_2 are measured as follows [15,16]:

$$S_0 = i_0 + i_{90}, \tag{1}$$

$$S_1 = i_0 - i_{90}, \tag{2}$$

$$S_2 = i_{45} + i_{35}, \tag{3}$$

where i_0, i_{45}, i_{90}, and i_{135} are the intensity values measured at the polarizer's four rotational positions 0°, 45°, 90°, and 135°, respectively.

An alternative and more intuitive representation of the incoherent monochrome radiation is the degree of linear polarization (DoLP). It can be calculated by the Stokes parameters as follows [16]:

$$\mathrm{DoLP} = \frac{\sqrt{S_1^2 + S_2^2}}{S_0}. \tag{4}$$

B. Imaging Spectropolarimeter

The imaging spectropolarimeter is schematically depicted in Fig. 1. An incoherent white light source (halogen light source) is used. The light is collimated by a 20 cm focal length lens and delivered to the skin at an angle of 25° to the normal of the skin surface. The choice of angle is not critical, and oblique angles of illumination other than 25° also work. The camera (Retiga Exi made by QImaging Corporation, 12 bit CCD camera), with a macro lens, collects only light that enters the skin and is backscattered toward the camera. A liquid crystal tunable filter (LCTF), made by Cambridge Research Instruments, is incorporated with a CCD to acquire the spectropolarimetric images. The full width at half-maximum has three options (7, 10, and 20 nm), which are set during the design and manufacturing process and cannot be adjusted by the end user. The spectral range of the LCTF is 400–720 nm.

The LCTF is a bandpass filter that can control the wavelength of the transmitting light. It is based on a multistage Lyot-type polarization interference filter with an electronically controllable liquid-crystal wave plate in each stage to provide variable

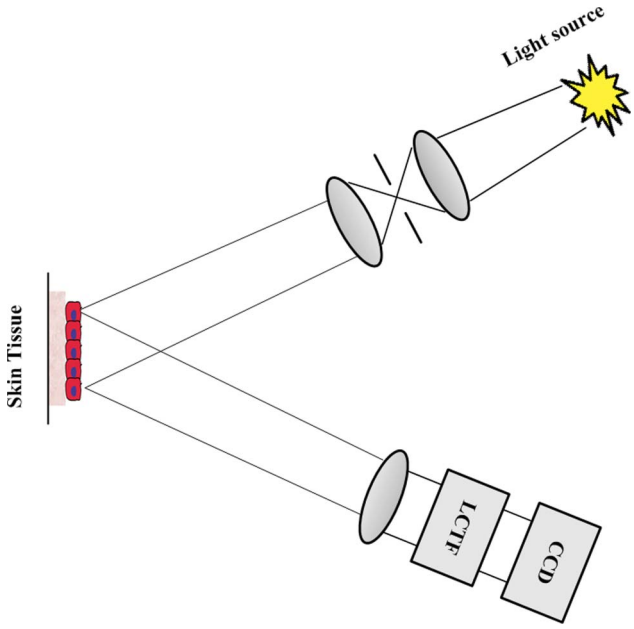

Fig. 1. (Color online) Illustration of the established spectropolarimetric imaging system. The spectral range from 400 to 720 nm. There are a total of 32 spectral bands with 10 nm space between each band. The linear polarization characteristics—intensity, the degree of linear polarization, and the phase of polarization at each band—can be acquired.

retardance. The configuration of the LCTF is shown in Fig. 2. A linear polarizer is included in the filter that allows the transmission of only the associated polarized component. The percentage of linearly polarized light, oriented so that maximum transmission is attained, passing through the filter relative to the amount that entered, is shown in Fig. 3. In the imaging system, the LCTF in front of the camera is manually aligned at four different angles: 0°, 45°, 90°, and 135°. Four image sequences are acquired at each band, $i_{0,\lambda}$, $i_{45,\lambda}$, $i_{90,\lambda}$, and $i_{135,\lambda}$, where $\lambda = 1, 2, \ldots, K$ is the number of bands.

Fig. 2. (Color online) Configuration of LCTF. It has six stages, each of which consists of polarizer (a), fixed retarder (c), and liquid crystal elements (b).

The system is operated using a personal computer running the Windows operating system. A set of software was developed to control the instrument driver routines for the CCD detector. The software allows the user to select experimental parameters such as the CCD detector shutter exposure time. The structure of the spectropolarimetric imaging system and the associated image analysis procedures are shown in Fig. 4. An example of the six band intensity images (530, 560, 590, 620, 650, and 680 nm) collected by the CCD detector is shown in Fig. 5. There is a progression from dimmer images to brighter images because of the light source's spectrum shape. In order to compute the wavelength dependence of the skin, it is necessary to normalize the images to eliminate the effect of the light source shape. The calculated polarimetric images (S_0, S_1, S_2, and DoLP) in the 590 nm band are shown in Fig. 6.

C. Spectropolarimetric Correction

In the imaging process, the sensed light contains not only light scattered by tissues but also light scattered/reflected by surroundings. The spectral channels have unknown gains due to filter transmission and CCD response and have unknown offsets

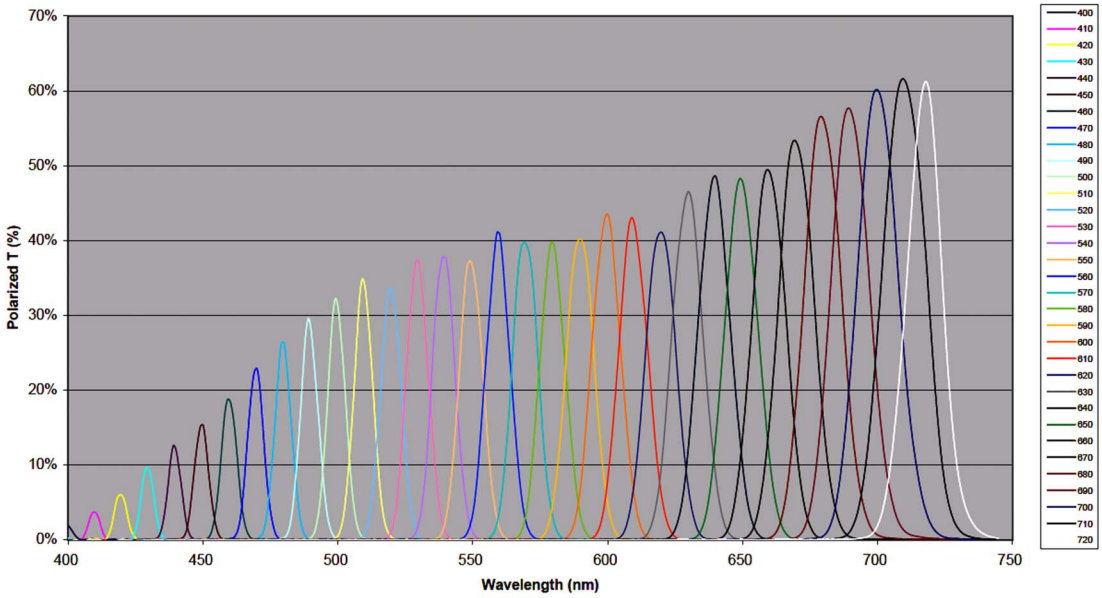

Fig. 3. (Color online) Percentage of linearly polarized light, oriented so that maximum transmission is attained, passing through the filter relative to the amount that entered.

due to dark current. These images must be corrected to make the acquired spectropolarimetric information more precise. Therefore, we propose a method to convert the raw images into spectropolarimetric reflectance images for analysis. Two Spectralon panels and a spectrometer (GER 2600, spectral range of 350–1050 nm, bandwidth of 1.5 nm) are used in calibration [17]. The panel, with approximately 99% reflectance, is referred to as white Spectralon, and a panel with lower than 5% and symmetrical reflectance is referred to as black Spectralon. Their reflectance is measured by the spectrometer and represented as R_w and R_b, respectively.

The raw measurement obtained by the imaging spectropolarimeter at spatial coordinate (x,y) and wavelength λ in direction α is given by

$$\mathrm{DN}(x,y,\lambda,\alpha) = t(x,y,\lambda,\alpha)R(x,y,\lambda,\alpha) + O(x,y,\lambda,\alpha), \tag{5}$$

where $t(x,y,\lambda,\alpha)$ is the illumination, the system spectral response $R(x,y,\lambda,\alpha)$ is the reflectance of the viewed surface, and $O(x,y,\lambda,\alpha)$ is the offset, which includes dark current and stray light. Here we suppose that $t(x,y,\lambda,\alpha)$ and $O(x,y,\lambda,\alpha)$ are constant for the imaging system at wavelength λ in direction α, so that $t(x,y,\lambda,\alpha)$ and $O(x,y,\lambda,\alpha)$ can be estimated by the spectropolarimetric response of white Spectralon and black Spectralon. For the image of white Spectralon, we have

$$\mathrm{DN}_w(x,y,\lambda,\alpha) = t(x,y,\lambda,\alpha)R_w(\lambda,\alpha) + O(x,y,\lambda,\alpha), \tag{6}$$

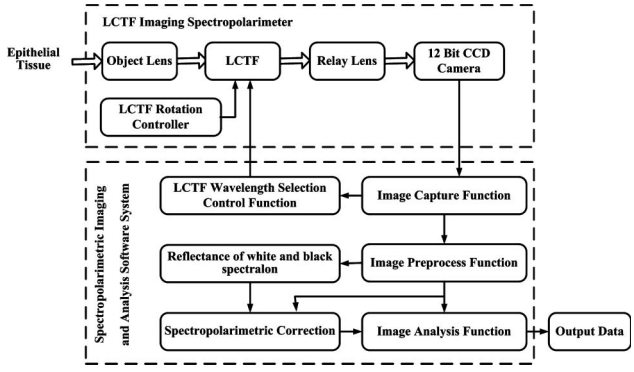

Fig. 4. Structure of the spectropolarimetric imaging and analysis system.

and for the image of black Spectralon, we have

$$\mathrm{DN}_b(x,y,\lambda,\alpha) = t(x,y,\lambda,\alpha)R_w(\lambda,\alpha) + O(x,y,\lambda,\alpha). \tag{7}$$

From Eqs. (6) and (7), we can estimate the $t(x,y,\lambda,\alpha)$ and $O(x,y,\lambda,\alpha)$ [8,17]. With these estimates, the reflectance can be given by

$$R(x,y,\lambda,\alpha) = \frac{(\mathrm{DN}(x,y,\lambda,\alpha) - \mathrm{DN}_b(x,y,\lambda,\alpha))R_w(\lambda,\alpha) + (\mathrm{DN}_w(x,y,\lambda,\alpha) - \mathrm{DN}(x,y,\lambda,\alpha))R_b(\lambda,\alpha)}{\mathrm{DN}_w(x,y,\lambda,\alpha) - \mathrm{DN}_b(x,y,\lambda,\alpha)}. \tag{8}$$

Then the reflectance of different Stokes parameters and DoLP at wavelength λ can be calculated as

$$R(x,y,\lambda,S_0) = R(x,y,\lambda,0°) + R(x,y,\lambda,90°), \tag{9}$$

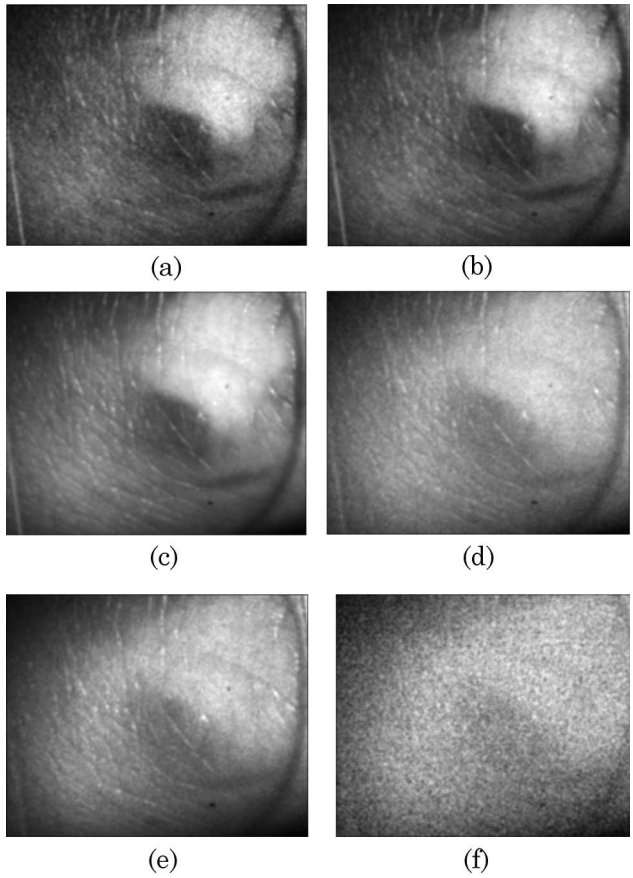

Fig. 5. Series of example skin images at different spectral bands: (a) 530 nm, (b) 560 nm, (c) 590 nm, (d) 620 nm, (e) 650 nm, (f) 680 nm.

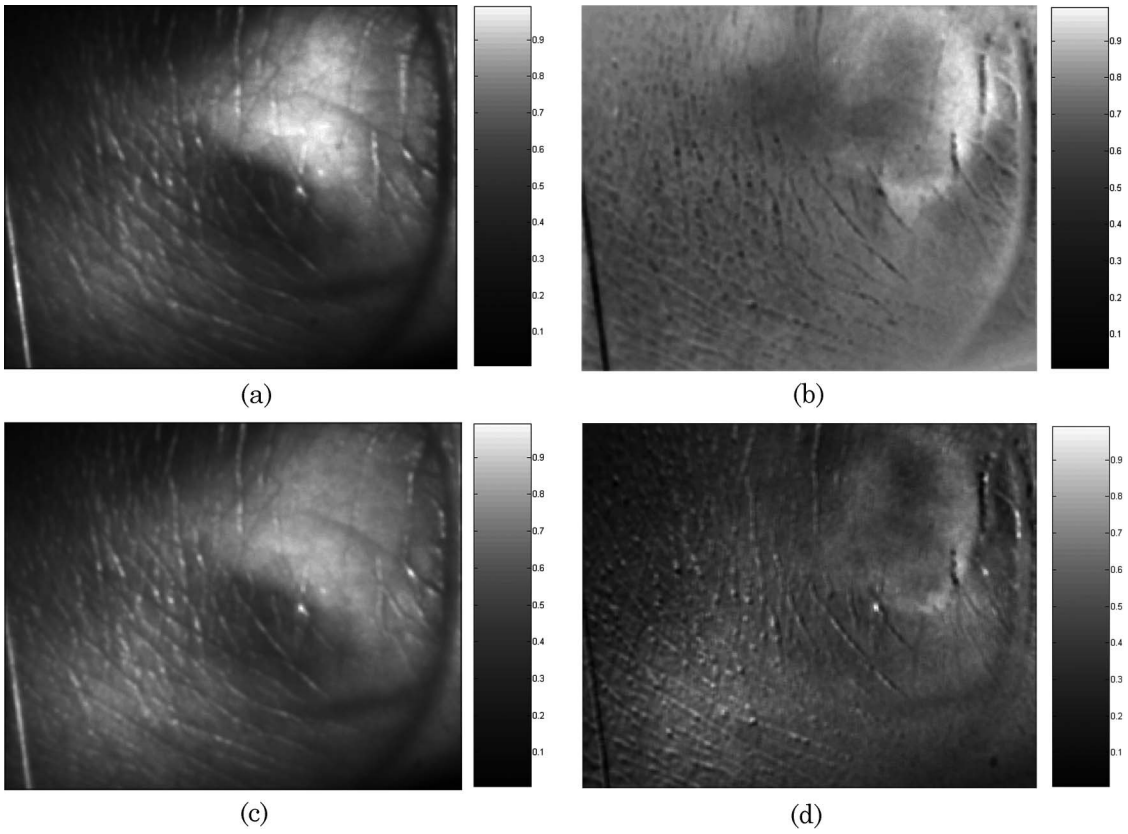

Fig. 6. Skin image described by different polarimetric parameters at 590 nm: (a) S_0, (b) S_1, (c) S_2, (d) DoLP.

$$R(x,y,\lambda,S_1) = R(x,y,\lambda,0^\circ) - R(x,y,\lambda,90^\circ), \quad (10)$$

$$R(x,y,\lambda,S_2) = R(x,y,\lambda,45^\circ) - R(x,y,\lambda,135^\circ), \quad (11)$$

$$R(x,y,\lambda,\mathrm{DoLP}) = \frac{\sqrt{R(x,y,\lambda,S_1)^2 + R(x,y,\lambda,S_2)^2}}{R(x,y,\lambda,S_0)}. \quad (12)$$

D. Visual Enhancement Algorithm

It is crucial to point out the pathological tissue region clearly and show its boundary accurately for computer-aided clinical diagnosis. As mentioned in Section 1, light-scattering spectrum and polarization states can provide different structural and functional information about the biological tissues. The Stokes parameter $S_{0,\lambda}$ gives the intensity of the beam at wavelength λ, and it can be used to describe the tissue's spectral characteristics. The spectral difference between the normal tissue and the pathological tissue across the bands is shown in Fig. 7(a). DoLP reflects the proportion of linear polarization energy in the whole beam's energy, and it can be used to describe the tissue's polarimetric characteristics. Figure 7(d) shows the polarimetric difference between the normal tissue and the pathological tissue across the bands.

On the other hand, there are some differences of spatial characteristics among Stokes parameters and DoLP. These differences can be observed in Fig. 6. The S_0 image contains more abundant texture information than the S_1, S_2, and DoLP images. The DoLP image has an advantage in describing the polarimetric difference. By exploiting more information about the objects of interest, better identification performance can be achieved. If the S_0 image can be fused with the DoLP images, an image with better contrast and more detailed textures can be expected. We propose here a false color mapping [15,18,19] based spectropolarimetric imagery fusion method to exploit the information from both the spectrum and the polarization states. It can integrate the texture information from the high spatial resolution S_0 image with the polarimetric information from the low spatial resolution DoLP images in different bands to achieve better discriminability of different pathological regions. The fusion algorithm is named spectropolarimetric false color image fusion, which is described as follows.

Algorithm of spectropolarimetric false color image fusion

1. The preprocessing, including denoising and normalization, is applied to the S_0 and DoLP image sequences.

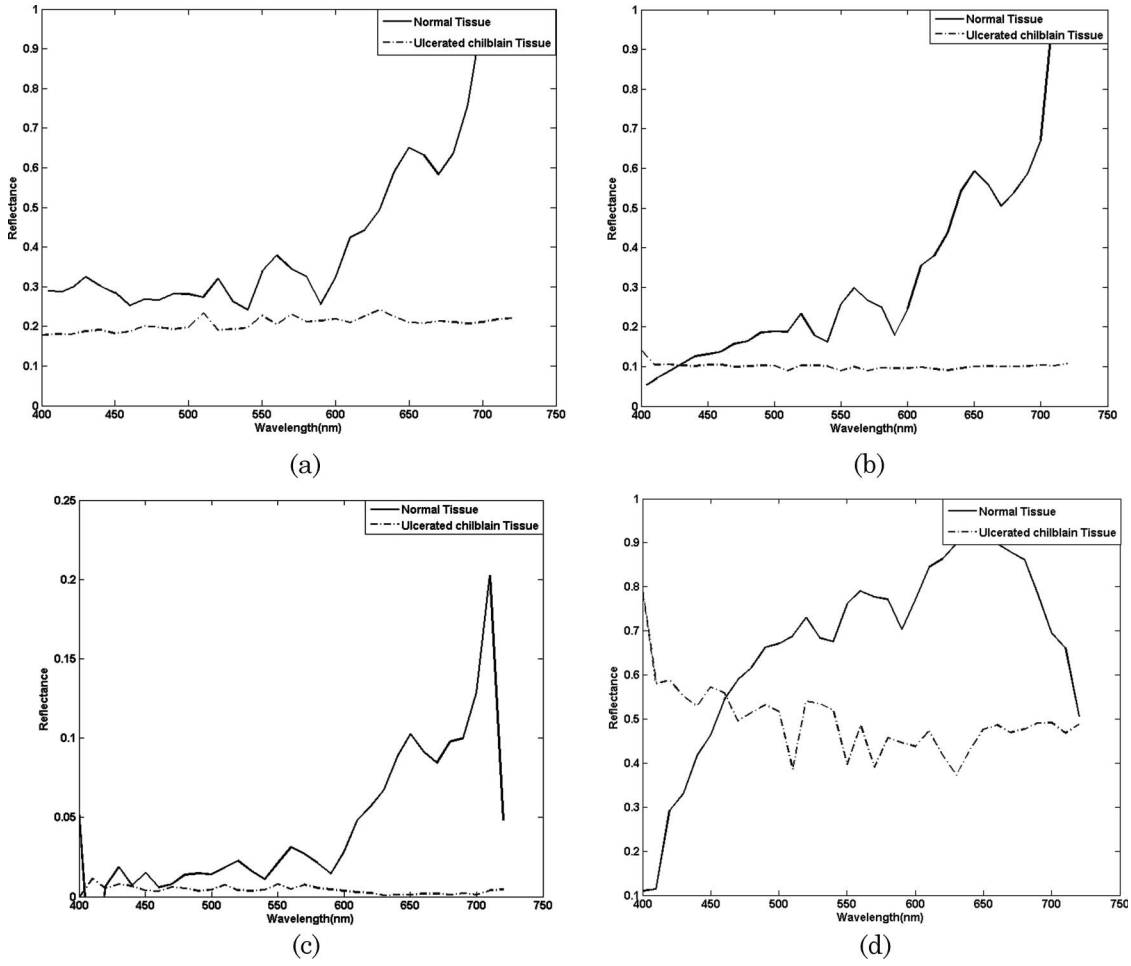

Fig. 7. Reconstructed spectropolarimetric curves of normal tissue and chilblain tissue: (a) S_0, (b) S_1, (c) S_2, and (d) DoLP. The x coordinate represents wavelength, and the y coordinate represents reflectance.

2. Principal component analysis (PCA) [20] is applied to the S_0 image sequence and the DoLP image sequence. We use the S_0 image sequence to illustrate the process, and the same procedure is applied to the DoLP sequence. Suppose there are N images in the S_0 image sequence and denote by $S_{0,n}$, $n = 1, 2, \ldots, N$, the column vector that contains all the pixels in the nth image. Then the S_0 image sequence can be represented in a matrix form: $\mathbf{S}_0 = [\vec{S}_{0,1}, \ldots, \vec{S}_{0,n}, \ldots \vec{S}_{0,N}]$. The covariance matrix of $\mathbf{S}_0$ is

$$\mathbf{\Omega} = \frac{1}{N}\mathbf{S}_0\mathbf{S}_0^T. \tag{13}$$

Let and r_i and $\vec{e}_i$ be the ith eigenvalue and the associated eigenvector of the covariance matrix $\mathbf{\Omega}$ and $r_1 \geq r_2 \geq \ldots \geq r_N$. We choose the first three eigenvectors $\vec{e}_1$, $\vec{e}_2$, and $\vec{e}_3$ that correspond to the first three most significant eigenvalues r_1, r_2, and r_3. Then we project $\mathbf{S}_0$ onto $\vec{e}_1$, $\vec{e}_2$, and $\vec{e}_3$ to obtain the first three most significant components as $\vec{S}_{0,\lambda_1} = \mathbf{S}_0 \cdot \vec{e}_1$, $\vec{S}_{0,\lambda_2} = \mathbf{S}_0 \cdot \vec{e}_2$, and $\vec{S}_{0,\lambda_3} = \mathbf{S}_0 \cdot \vec{e}_3$. Reformatting the three vectors into a 2D image format results in three images: S_{0,λ_1}, S_{0,λ_2}, and S_{0,λ_3}. Similarly, we can obtain $\mathrm{DoLP}_{\lambda 1}$, $\mathrm{DoLP}_{\lambda 2}$, and $\mathrm{DoLP}_{\lambda 3}$ for the DoLP image sequence.

3. Find the common spectral information in S_{0,λ_1}, S_{0,λ_2}, and S_{0,λ_3}:

$$\mathrm{Co}_{S_0} = S_{0,\lambda_1} \cap S_{0,\lambda_2} \cap S_{0,\lambda_3}, \tag{14}$$

where $A(i,j) \cap B(i,j) = \min\{A(i,j), B(i,j)\}$ [A and B represent digital images, and (i,j) represents the pixel coordinate].

4. Find the common polarimetric information in $\mathrm{DoLP}_{\lambda_1}$, $\mathrm{DoLP}_{\lambda_2}$, and $\mathrm{DoLP}_{\lambda_3}$:

$$\mathrm{Co}_{\mathrm{DoLP}} = \mathrm{DoLP}_{\lambda_1} \cap \mathrm{DoLP}_{\lambda_2} \cap \mathrm{DoLP}_{\lambda_3}. \tag{15}$$

5. Calculate the unique part in each image:

$$\begin{aligned} \mathrm{DoLP}^* &= \mathrm{DoLP}_{\lambda_1} - \mathrm{Co}_{\mathrm{DoLP}}, \\ S_0^* &= S_{0,\lambda_1} - \mathrm{Co}_{S_0}. \end{aligned} \tag{16}$$

The pairwise subtraction of multiband images can be used to enhance the difference between them. In Eqs. (16), through subtraction of the common

component, the unique information will be enhanced in each image.

6. Adjust the images by using the unique components:

$$\mathrm{DoLP}^{*} = \mathrm{DoLP}_{\lambda_1} - \mathrm{Co}_{\mathrm{DoLP}} - S_0^{*},$$
$$S_0^{**} = S_{0,\lambda_1} - S_0^{*}. \tag{17}$$

The unique components calculated by Eqs. (17) are subtracted from the original image of other modalities. This step serves to enhance the representation of each modality's specific details in the final fused result.

7. The resulting images can then be combined into a composite false color image by representing the processed S_0^{**} image as the red channel, the DoLP^{**} image as the green channel, and the S_0^{*} image as the blue channel of a red-green-blue (RGB) display:

$$\begin{pmatrix} R \\ G \\ B \end{pmatrix} = \begin{pmatrix} S_0^{**} \\ \mathrm{DoLP}^{**} \\ S_0^{*} \end{pmatrix}. \tag{18}$$

E. Example

In this subsection we use an example to illustrate the proposed spectropolarimetric false color image fusion process. Figure 8(a) shows an image that contains the common spectral information from the first three PCA components of the S_0 image sequence. Figure 8(b) shows an image that contains the common polarimetric information from the first three PCA components of the DoLP image sequence. The results of Eqs. (14) to (18) are shown in Figs. 8(c) and 8(d), and these two images demonstrate that pairwise subtraction of multiband images can be used to enhance the difference between them. Figures 8(e) and 8(f) show the unique components calculated by Eq. (17). We see that the specific details of each modality are enhanced. Figure 8(g) shows the final fusion results, and Fig. 8(h) shows the spectral image at 590 nm. By comparing Figs. 8(g) and 8(h), it can be concluded that it is much easier to separate the pathological tissue (highlighted in red online) in Fig. 8(g) by using the proposed method. The pathological tissue region is enhanced, and its boundary can be clearly identified. This is very helpful in computer-aided diagnosis to improve clinical diagnosis accuracy.

3. Experimental Results and Discussion

To document the performance of the proposed method, we applied it to the images collected from the forearms of 10 volunteer subjects with two different tissues: ulcerated chilblain and benign pigmented nevus. Figure 6 shows the polarimetric images S_0, S_1, S_2, and DoLP at 590 nm (ulcerated chilblain). Figure 7 shows the spectropolarimetric difference of ulcerated chilblain tissue and ambient normal tissue. It can be concluded that the spectropolarimetric differences of these two types of tissues change with the variation of wavelength. S_0 is equivalent to the total reflectance. S_1 represents the difference in intensity between horizontal and vertical linearly polarized components. S_2 is the difference between linearly polarized components oriented at $+45°$ and $-45°$. By comparing S_0, S_1, and S_2 images, it can be seen that there is a great increase of gray level difference between ulcerated chilblain and normal tissue due to the skin's superficial scattering of incident polarized light. DoLP is the combination of S_0, S_1, and S_2, and it emphasizes the scattering of incident polarized light by superficial tissues.

The S_0 image shows the ulcerated chilblain region as a slightly darker region due to the darker color of ulcerated chilblain. However, the S_1, S_2, and DoLP images show this region as a darker signal than normal skin. The collagen fibers in the ulcerated chilblain randomize the polarized illumination faster than they backscatter the polarized illumination. The balance between the rate of randomization and the rate of backscattering may be influenced by the size of collagen fiber bundles in the ulcerated chilblain. The S_1, S_2, and DoLP images can reveal some structural information about the ulcerated chilblain, suggesting that they could be helpful in evaluating the topography of ulcerated chilblain. The curves of these polarimetric parameters versus wavelength dependency are shown in Fig. 7.

Figure 8(h) shows the reflectance images at 590 nm, and Fig.8(g) shows the visual enhancement result, where the ulcerated chilblain region is shown in red online. Although the reflectance difference between ulcerated chilblain and normal tissue is obvious as shown in Fig. 7(a), it is difficult to determine the range of the ulcerated chilblain region. On the other hand, the ulcerated chilblain affects not only the skin vasculature but also the collagen fibers, while collagen fibers can rapidly depolarize the incident light [21]. Through fusing the information provided by spectral and polarimetric images, better contrast can be obtained. In the fusion, both the spectral difference and polarimetric difference between ulcerated chilblain and normal tissue are exploited. Comparing Figs. 8(a) and 8(b), it can be clearly seen that the boundary between these two tissues is much enhanced.

Figure 9 shows four benign pigmented nevus regions, marked by four circles, 1, 2, 3, and 4. The pigmented nevus 2 and 3 can be obviously seen in the spectral images because of their black color; however, pigmented nevus 1 and 4 are relatively unclear. In the S_0 image at 590 nm, the fourth pigmented nevus can be observed, while there is some confusion of the locations of the benign pigmented nevus regions in the DoLP image. This is mainly due to the influence of collagen fibers. On the other hand, the difference between the nevus and the normal tissue

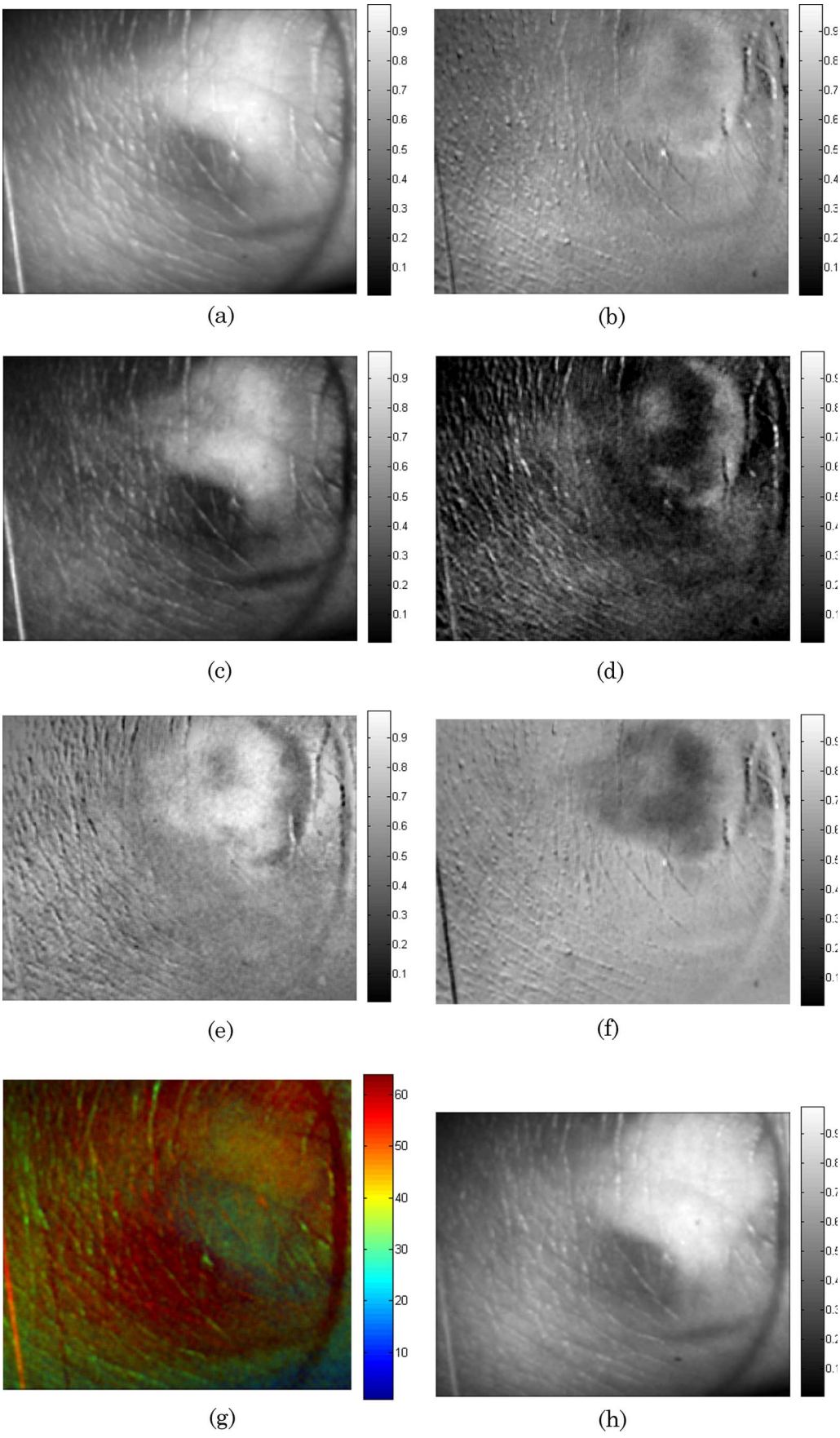

Fig. 8. (Color online) Example of the spectropolarimetric false color image fusion process: (a) image of Co_{S_0}, (b) image of Co_{DoLP}, (c) image of DoLP*, (d) image of S_0^*, (e) image of S_0^{**}, (f) image of DoLP $**$, (g) visually enhanced result, (h) reflectance image of chilblain at 590 nm.

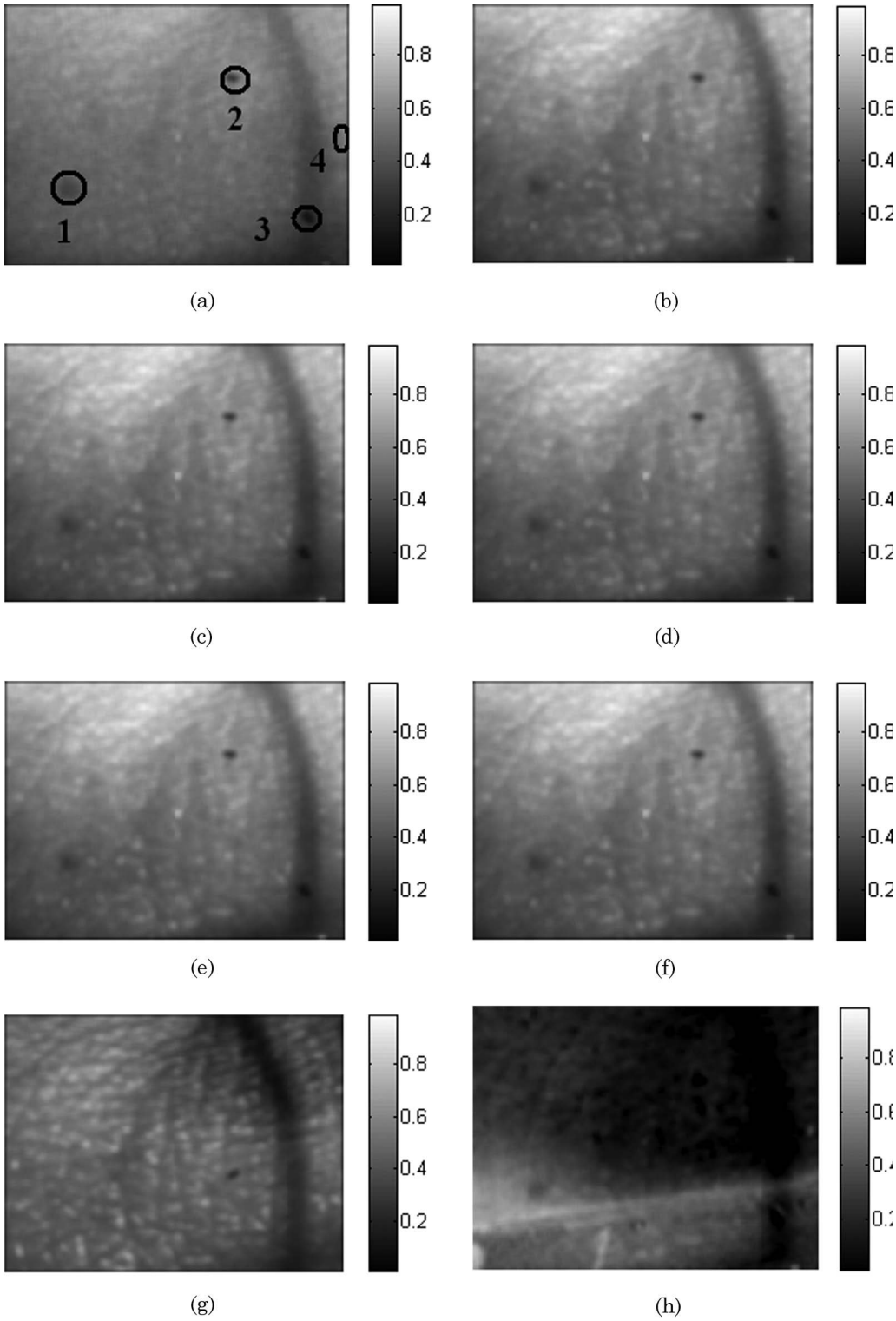

Fig. 9. Benign pigmented nevus images at intensities of (a) 560 nm, (b) 590 nm, (c) 620 nm, (d) 650 nm, (e) S_0 image at 590 nm, (f) S_1 image at 590 nm, (g) S_2 image at 590 nm, and (h) DoLP image at 590 nm.

becomes more and more obvious with the increase of wavelength. This is because the spectral reflectance is sensitive to the variation of melanosomes, as shown in Figs. 10(a) and 10(b). From Figs. 10(a) and 10(b), it can be observed that the spectral difference from 500 to 600 nm is relatively small but the DoLP difference is much more obvious.

Figure 11(a) shows the reflectance image at 590 nm, where the brown pigmented nevus is almost invisible. Figure 11(b) shows the visual enhancement

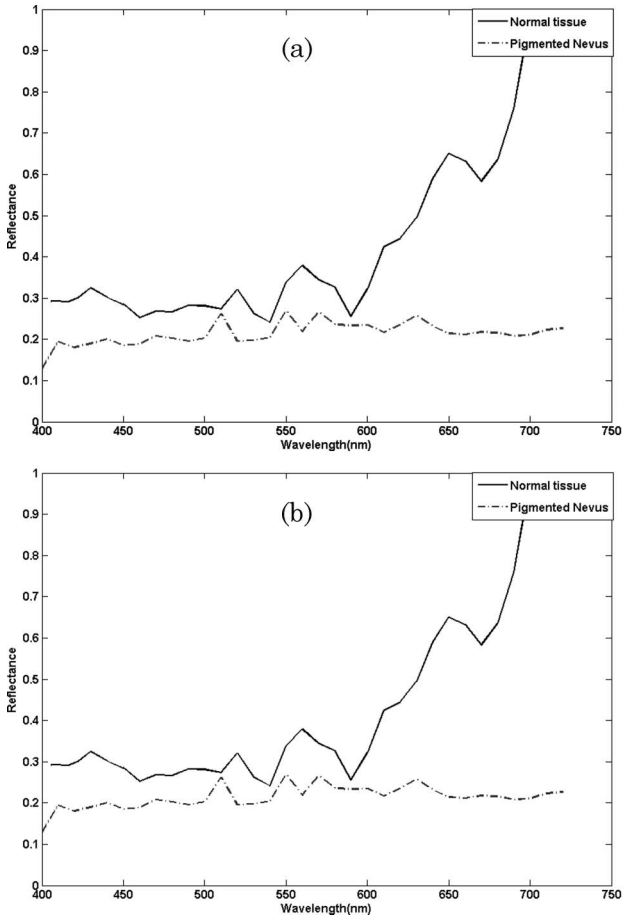

Fig. 10. Reconstructed spectropolarimetric curves of normal tissue and benign pigmented nevus: (a) S_0,(b) DoLP. The x coordinate is the wavelength, and the y coordinate is reflectance.

result of melanin, where the pigmented nevus is shown in black and the surrounding skin is shown in green online. By comparing Figs. 11(a) and 11(b), it is seen that through spectropolarimetric image fusion, the boundary of benign pigmented nevus can be much better determined. It is very desirable in monitoring the variation of the size of pigmented nevus.

The two different tissues in the experiment contain vasculature, collagen fibers, and melanin structures, and they will change the light-scattering spectra and polarization states. Vasculature, collagen, and melanin are typical structures of cancer [4,22,23]. Cancer tends to result in the denaturization of the collagen, thus resulting in a loss of birefringence due to the deformation of the regular molecular binding structure [22], and light-scattering polarization states will also be changed according to the variation of birefringence. At the same time, the variation of melanin and vasculature will change the light-scattering spectra [23]. Through spectropolarimetric false color image fusion, the spectral and polarimetric difference can be utilized jointly, and the difference of normal tissue and pathological tissue can be enhanced. This can benefit the detection and identification of pathological tissues.

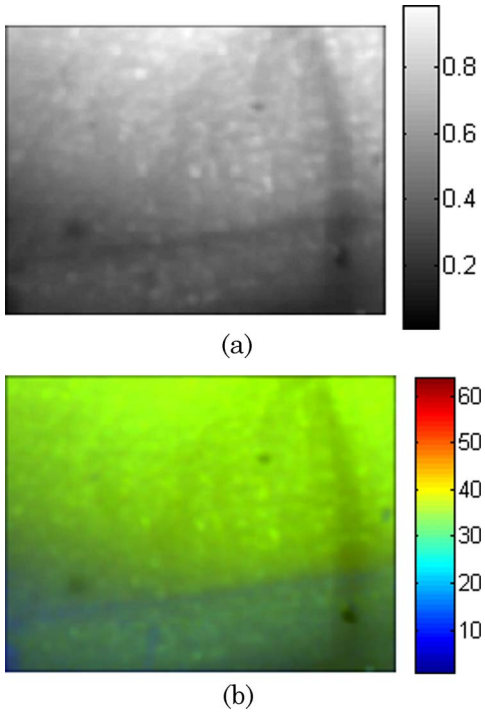

Fig. 11. (Color online) (a) Reflectance image of benign pigmented nevus at 590 nm, (b) visually enhanced result of (a).

4. Conclusion

We have reported a new spectropolarimetric imaging method for analysis of tissue characteristics and proposed a visual enhancement method to fuse the acquired spectral and polarimetric information by using false color mapping. The experimental results show that spectropolarimetric imaging can be used to discriminate the different pathological tissues efficiently. The spectral and polarimetric information can reveal biochemical and structural information about the tissue. The proposed visual enhancement algorithm provides an intuitive and obvious clue of the pathological tissue region for computer-aided diagnosis.

This work is supported by the National Natural Science Foundation of China (NSFC) under grants 60602056 and 60634030 and the China Scholarship Council under 200521s073.

References

1. V. Backman, R. Gurjar, K. Badizadegan, I. Itzkan, R. Dasari, L. Perelman, and M. Feld, "Polarized light scattering spectroscopy for quantitative measurement of epithelial cellular structures in situ," IEEE J. Sel. Top. Quantum Electron. **5**, 1019–1026 (1999).
2. R. S. Gurjar, V. Backman, L. T. Perelman, I. Georgakoudi, K. Badizadegan, I. Itzkan, R. Dasari, and M. Feld,"Imaging human epithelial properties with polarized lightscattering spectroscopy," Nat. Med. **7**, 1245–1248 (2001).
3. S. L. Jacques, J. C. Ramella-Roman, and K. Lee, "Imaging skin pathology with polarized light," J. Biomed. Opt. **7**, 329–340 (2002).

4. G. L. Liu, Y. F. Li, and B. D. Cameron, "Polarization-based optical imaging and processing techniques with application to the cancer diagnostics," Proc. SPIE **4617**, 208–220 (2002).
5. S. L. Jacques, J. R. Roman, and K. Lee, "Imaging superficial tissues with polarized light," Lasers Surg. Med. **26**, 119–129 (2000).
6. R. Riddell, H. Goldman, D. Ransohoff, H. Appelman, C. Fenoglio, R. Haggitt, C. Ahren, P. Correa, S. Hamilton, and B. Morson, "Dysplasia in inflammatory bowel-disease, standardized classification with provisional clinical-applications," Human Pathol. **14**, 931–968 (1983).
7. J. R. Mourant, I. J. Bigio, J. Boyer, L. Richard, J. Tamara, and S. Tsutomu, "Spectroscopic diagnosis of blader cancer with elastic light scattering," Laser Surg. Med. **7**, 350–357 (1995).
8. T. Shi and C. A. Dimarzio, "Multispectral method for skin imaging: development and validation," Appl. Opt. **46**, 8619–8626 (2007).
9. G. N. Stamatas, C. Balasb, and N. Kollias, "Hyperspectral image acquisition and analysis of skin," Proc. SPIE **4959**, 77–82 (2003).
10. T. Vo-Dinh, D. L. Stokes, M. B. Wabuyele, M. Martin, J. Song, R. Jagannathan, E. Michaud, R. Lee, and X. Pan, "A hyperspectral imaging system for in vivo optical diagnostics," IEEE Eng. Med. Biol. Mag. **23**, 40–49 (2004).
11. L. Perelman, "Polarized light scattering spectroscopy of epithelial structures," in *Conference on Lasers and Electro-Optics* (Optical Society of America, 2000), pp. 530–531.
12. G. Jarry, E. Steimer, V. Damaschini, M. Epifanie, M. Jurczak, and R. Kaiser, "Coherence and polarization of light propagating through scattering media and biological tissues," Appl. Opt. **37**, 7357–7367 (1998).
13. D. Manolakis, D. Marden, and G. A. Shaw, "Hyperspectral image processing for automatic target detection applications," Lincoln Lab. J. **14**, 79–100 (2003).
14. J. R. Schott, *Remote Sensing: The Image Chain Approach* (Cambridge U. Press), Chap.1, pp. 13–17 .
15. Y. Zhao, Q. Pan, and H. Zhang, "New polarization imaging method based on spatially adaptive wavelet image fusion," Opt. Eng. **44**, 123202 (2006).
16. D. Goldstein, *Polarized Light*, 2nd ed. (Marcel Dekker, 2003), pp. 31–63, pp. 133–145.
17. Z. Pan, G. Healey, M. Prasad, and B. Tromberg, "Face recognition in hyperspectral images," IEEE Trans. Pattern Anal. Mach. Intell. **25**, 1552–1560 (2003).
18. G. Pajares and J. Manuel de la Cruz, "A wavelet-based image fusion tutorial," Pattern Recogn. **37**, 1855–1872 (2004).
19. 'A. Toet and J. Walraven, "New false color mapping for image fusion," Opt. Eng. **35**, 650–658 (1996).
20. I. T. Jolliffe, *Principal Component Analysis*, 2nd ed. (Springer-Verlag, 2002), Chap. 6, pp. 111–130.
21. M. Manabu, "Past history and occurrence patterns of chilblain in collagen diseases," Nishinihon J. Dermatol. **6**, 736–741 (2002).
22. A. M. P. Montgomery, R. A. Reisfeld, and D. A. Cheresh, "Integrin aVP3 rescues melanoma cells from apoptosis in three-dimensional dermal collagen," Proc. Natl. Acad. Sci. USA **91**, 8856–8860 (1994).
23. M. Tercelj, T. Rott, D. Reinders, and Y. Fawzy, "Spectral bronchoscopy for evaluation of tissue vascular properties in lung cancer," http://www.perceptronix.com/news/Publications/ERSPresentation_%2009062007.pdf.